Wavelength Selection for Synthetic Image Generation

Gary W. Meyer

CIS-TR-87-14
November 16, 1987

To appear in *Computer Vision, Graphics and Image Processing*

Work originally performed at the Program of Computer Graphics,
Cornell University

Department of Computer and Information Science
University of Oregon

1. Introduction

Sophisticated lighting models employed in computer graphics today synthesize color by computing spectral energy distributions on a wavelength by wavelength basis (Cook and Torrance [1], Hall and Greenberg [2]). Reflectances are assigned to materials, emittances are associated with light sources, and models of how light interacts with matter are used to determine the spectral energy distributions that would reach an observer of the scene. These spectral energy distributions are converted to tristimulus values by using the principles of color science. Finally, these color coordinates are transformed into a set of tristimulus values appropriate for a particular color reproduction device.

There are several objectives to be met in performing these calculations. Although any linear transform of the human spectral sensitivities defines a valid color space in which to represent the tristimulus values, a color space should be chosen which minimizes any errors that might be inherent in the computations. Furthermore, since the lighting model calculations may have to be repeated for every wavelength used, the minimum number of wavelengths necessary to insure adequate color fidelity should be employed to represent the spectral energy distribution. In addition, the wavelengths used should be spaced across the visible spectrum so that they are located at the positions most important for accurate color rendition.

This paper shows how gaussian quadrature with a set of opponent fundamentals can be used to select the wavelengths at which to perform synthetic image generation. First a set of opponent fundamentals are derived from the CIE XYZ matching functions and are shown to be the basis for an optimal color space in which to perform color synthesis calculations. Next the wavelengths at which to conduct realistic image synthesis are selected via gaussian quadrature with the opponent fundamentals as weighting functions. Finally,

this wavelength selection technique is evaluated by color difference calculations on a set of representative spectral energy distributions and by a perceptual comparison experiment between a real scene and a computer generated picture of that scene.

2. An Optimal Color Space for Color Synthesis

The color space that is employed for color synthesis work should be selected so as to minimize any errors inherent in the computation. The fundamental spectral sensitivity functions of the human visual system are what all color reproduction techniques are based upon. They are introduced in the following subsection. However, the color space that is formed by the fundamental spectral sensitivity functions is not optimal from the standpoint of color synthesis work. In the second subsection, the results of Buchsbaum and Gottschalk [3] are used to derive an opponent representation of these fundamentals by the use of the Karhunen-Loeve expansion. The color space that results from this transformation minimizes the error of representation for the tristimulus values and hence reduces the errors that occur in color synthesis calculations.

2.1 The fundamental spectral sensitivities

The fundamental spectral sensitivities of the human visual system form the basis for any color calculations in realistic image synthesis. Given the 1931 CIE standard observer matching functions ($\overline{x}(\lambda)$, $\overline{y}(\lambda)$, and $\overline{z}(\lambda)$), a set of dichromatic confusion loci, and a method for establishing the relative sensitivity of the resulting functions, the following definition of the fundamental spectral sensitivities (Fig. 1) can be derived

$$\begin{bmatrix} \overline{s}(\lambda) \\ \overline{m}(\lambda) \\ \overline{l}(\lambda) \end{bmatrix} = \begin{bmatrix} 0.0000 & 0.0000 & 0.0127 \\ -0.2606 & 0.7227 & 0.0562 \\ 0.1150 & 0.9364 & -0.0203 \end{bmatrix} \begin{bmatrix} \overline{x}(\lambda) \\ \overline{y}(\lambda) \\ \overline{z}(\lambda) \end{bmatrix} \tag{1}$$

The details of this derivation can be found in Appendix A.. The S, M, and L tristimulus values are determined for a spectral energy distribution $E(\lambda)$ by

$$\begin{aligned} S &= \int_{380}^{770} E(\lambda)\overline{s}(\lambda)\,d\lambda \\ M &= \int_{380}^{770} E(\lambda)\overline{m}(\lambda)\,d\lambda \\ L &= \int_{380}^{770} E(\lambda)\overline{l}(\lambda)\,d\lambda \end{aligned} \tag{2}$$

where 380 nm and 770 nm are taken as the limits of the visible spectrum in this paper. Figure 2 shows an SML coordinate system and the cone of realizable color that forms the boundary of all possible tristimulus values.

2.2 The opponent spectral sensitivities

In order to minimize the effect of any errors that might happen while synthesizing colors, the axes of the color space which is used to perform the calculations should be oriented so that they pass through the regions where tristimulus values are most likely to occur. In addition to being limited to a particular region of color space, the SML tristimulus values determined in Eq. (2) are not evenly distributed throughout the cone of realizable color. The fact that the $\overline{m}(\lambda)$ and $\overline{l}(\lambda)$ spectral sensitivities in Fig. 1 overlap each other to such a great extent but hardly overlap the $\overline{s}(\lambda)$ spectral sensitivity at all means that the M and L portions of a tristimulus value will always be highly correlated with each other but will not be correlated with the S portion of a tristimulus value. This can be seen in Fig. 2 where the locus for the equal energy spectral energy distribution makes two major loops: one loop in the LM plane at a 45 degree angle to the L and M axes and one loop in the direction of the

S axis. If it is assumed that relatively smooth spectral energy distributions are more likely to occur than spikey spectral energy distributions, then tristimulus values at the boundary of the cone where monochromatic lights are represented are less probable than tristimulus values in the interior of the cone. A transform of the SML coordinate system should be sought which directs the axes through the most dense regions of tristimulus values and which assigns a priority to each axis depending on the proportion of the coordinates which lie along its direction.

The discrete Karhunen-Loeve expansion can be used to find such a transform. The application of this technique to the study of human color vision was first performed by Buchsbaum and Gottschalk [3,4]. The new coordinates A, C_1, and C_2 which result from the transformation

$$\begin{bmatrix} A \\ C_1 \\ C_2 \end{bmatrix} = \begin{bmatrix} \\ T \\ \\ \end{bmatrix} \begin{bmatrix} S \\ M \\ L \end{bmatrix} \tag{3}$$

should be prioritized in such a way that they can be distorted or even eliminated one by one with minimum impact on the mean squared error. It can be shown [5] that this will happen when the rows of the transformation matrix T are the eigenvectors of the covariance matrix

$$\begin{bmatrix} C_{SS} & C_{SM} & C_{SL} \\ C_{SM} & C_{MM} & C_{ML} \\ C_{SL} & C_{ML} & C_{LL} \end{bmatrix} \tag{4}$$

where

$$\begin{aligned} C_{SS} &= \iint K(\lambda,\mu)\overline{s}(\lambda)\overline{s}(\mu)\,d\lambda\,d\mu \\ C_{SM} &= \iint K(\lambda,\mu)\overline{s}(\lambda)\overline{m}(\mu)\,d\lambda\,d\mu \end{aligned} \tag{5}$$

with similar expressions for the other terms. $K(\lambda,\mu)$ is the covariance function and $\overline{s}(\lambda)$, $\overline{m}(\lambda)$, and $\overline{l}(\lambda)$ are the fundamental spectral sensitivities defined in Eq. (1). The eigenvalue

transformation from 1931 CIE XYZ space to the optimal AC_1C_2 space:

$$\begin{bmatrix} A \\ C_1 \\ C_2 \end{bmatrix} = \begin{bmatrix} -0.0177 & 1.0090 & 0.0073 \\ -1.5370 & 1.0821 & 0.3209 \\ 0.1946 & -0.2045 & 0.5264 \end{bmatrix} \begin{bmatrix} X \\ Y \\ Z \end{bmatrix} \tag{9}$$

The eigenvalue ratio is

$$102.4 \ : \ 2.29 \ : \ 0.0221 \tag{10}$$

between A, C_1, and C_2 respectively.

The prioritization of the coordinates indicated in Eq. (10) can be seen by comparing Fig. 3 of the new AC_1C_2 space with Fig. 2 of SML space. The A axis is roughly positioned along the line that lies at 45 degrees with respect to the L and M axes and thus passes through the most dense region of tristimulus values. This is because of the high correlation between the L amd M components of the tristimulus values. Although it is difficult to see in Fig. 3, the C_1 axis lies in the LM plane. Since it is perpendicular to the A axis which points in the direction of high L and M component correlation, the C_1 axis records the differences between the L and M components of the tristimulus values. The C_2 axis lies close to the S axis and thus primarily records the value of the relatively insensitive short wavelength receptor.

The $\overline{a}(\lambda)$, $\overline{c}_1(\lambda)$, and $\overline{c}_2(\lambda)$ sensitivities which correspond to the A, C_1, and C_2 coordinates are shown in Fig. 4. They are very similar in shape to many of the opponents fundamentals which have been proposed for the human visual system. The achromatic channel, designated as A, corresponds closely to the photopic luminous efficiency function $\overline{y}(\lambda)$. The chromatic channels, designated as C_1 and C_2, correspond to the red/green and yellow/blue functions of the classical opponent fundamentals. Buchsbaum and Gottschalk [3] were able to directly compare their fundamentals to those of Ingling [7] and Guth et.

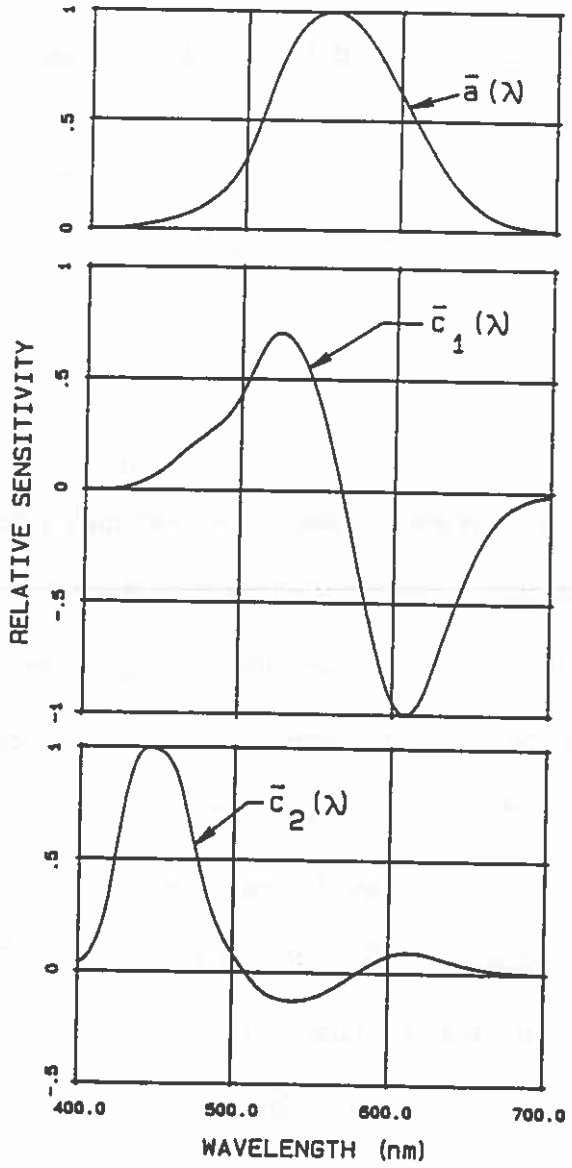

Figure 4: Spectral sensitivities for AC_1C_2 space.

The abscissas x_0, x_1, ..., x_n are found by use of the family of polynomials $P_n(x)$ orthogonal to $w(x)$ over the interval (a, b). If the inner product is defined as

$$\langle g, h \rangle = \int_a^b g(x)h(x)w(x)\,dx \tag{14}$$

then the orthogonality condition for the polynomials becomes

$$\langle P_n(x), P_m(x) \rangle = 0 \qquad (m \neq n; \quad m, n = 0, 1, 2, \ldots) \tag{15}$$

These polynomials can be found from the three term recurrence relation [12]

$$\begin{aligned} P_{k+1}(x) &= (x - A_k)P_k(x) - B_k P_{k-1}(x) \qquad (k = 0, 1, \ldots) \\ P_{-1}(x) &= 0 \\ P_0(x) &= 1 \end{aligned} \tag{16a}$$

where

$$\begin{aligned} A_k &= \frac{\langle xP_k(x), P_k(x) \rangle}{\langle P_k(x), P_k(x) \rangle} \qquad (k = 0, 1, \ldots) \\ B_k &= \frac{\langle P_k(x), P_k(x) \rangle}{\langle P_{k-1}(x), P_{k-1}(x) \rangle} \qquad (k = 1, 2, \ldots) \end{aligned} \tag{16b}$$

The abscissas x_0, x_1, ..., x_n are the zeros of the $n+1$ order orthogonal polynomial defined above.

If $w(x)$ is nonnegative on $(a,\ b)$, gaussian quadrature can be shown to have several important convergence and error properties. For $f(x)$ a polynomial of degree less than or equal to $2n\ +\ 1$, Eq. (12) is exact. If $f(x)$ is not such a polynomial but is still continous on $(a,\ b)$ (or even discontinous in certain cases) convergence is guaranteed in the limit as n goes to infinity [13]. In terms of error estimates, gaussian quadrature can be shown to be as good as any other quadrature formula that employs the same number of points [13]. This property is not affected by integrals which only have low order derivatives.

Many of the desirable properties of gaussian quadrature continue to hold if $w(x)$ assumes negative values on (a, b). The existence of the orthogonal polynomials $P_n(x)$ does not depend

order	A		C_1		C_2	
	λ_i	H_i	λ_i	H_i	λ_i	H_i
1	559.2	1.05638	undefined		456.4	0.54640
2	516.9 601.5	0.52827 0.52811	490.9 631.4	0.31824 -0.46008	444.0 631.6	0.51004 0.03636
3	483.0 557.7 632.3	0.15908 0.71695 0.18035	undefined		386.9 447.7 644.9	0.01859 0.49780 0.03001
4	457.6 529.3 592.5 660.5	0.04639 0.50400 0.46254 0.04346	450.8 509.9 618.4 679.3	0.04863 0.33007 -0.47764 -0.04290	undefined	
5	441.3 506.7 562.3 621.0 688.4	0.01727 0.25935 0.56306 0.20904 0.00766	undefined		undefined	
6	429.4 484.6 537.8 590.4 644.8 713.4	0.00697 0.10576 0.47284 0.39430 0.07519 0.00131	428.3 468.2 518.5 610.9 658.3 723.6	0.00607 0.08951 0.30806 -0.43681 -0.10674 -0.00193	undefined	
7	419.1 465.0 517.7 564.7 614.0 665.6 732.0	0.00261 0.04337 0.30092 0.47041 0.21567 0.02311 0.00030	undefined		401.2 433.3 466.4 546.5 618.3 664.7 729.5	0.01622 0.25009 0.27643 -0.04131 0.03706 0.00779 0.00013
8	409.6 450.0 499.3 543.0 588.1 634.2 684.4 744.4	0.00089 0.02039 0.15315 0.42595 0.34893 0.10036 0.00662 0.00010	407.3 443.1 481.0 524.3 605.5 645.7 693.1 748.3	0.00031 0.02106 0.11686 0.28008 -0.38470 -0.16389 -0.01134 -0.00022	undefined	

Table 1a: Wavelengths and weights necessary to compute AC_1C_2 tristimulus values using gaussian quadrature of orders one through eight.

4. Evaluation of Wavelength Selection Technique

A series of experiments was performed in order to evaluate the effectiveness of using gaussian quadrature to determine AC_1C_2 tristimulus values. In one set of tests, gaussian quadrature was used to compute tristimulus values for a representative set of spectral energy distributions. The color difference was then determined in a perceptually uniform color space between the actual and the computed tristimulus values for these spectral energy distributions. In another set of tests, gaussian quadrature was used to produce several computer generated pictures. These pictures were then compared against a model of a real scene.

4.1 Color Difference Calculations

The color difference calculations involved the computation of tristimulus values for the 24 color swatches in the Macbeth Color Checker chart. The reflectances of these swatches (Figs. 5a to 5g) are representative of commonly occurring reflectances (McCamy, Marcus, and Davidson [15]). CIE standard illuminant C was used as the light source in all of the tests. The color difference between the actual tristimulus values and those determined using various quadrature techniques were expressed as a distance in CIE $L^*a^*b^*$ space [16]. The nominally white object color stimulus was taken to be illuminant C in the computation of the $L^*a^*b^*$ coordinates.

The first test compared gaussian quadrature performed in the AC_1C_2 space defined by Eq. (9) against gaussian quadrature performed in CIE XYZ space and against gaussian quadrature performed in SML space defined by Eq. (1). The wavelengths and coefficients used to compute the AC_1C_2 tristimulus values are given in Tables 1a and 1b. For CIE XYZ space and SML space, the gaussian wavelengths and coefficients were computed by

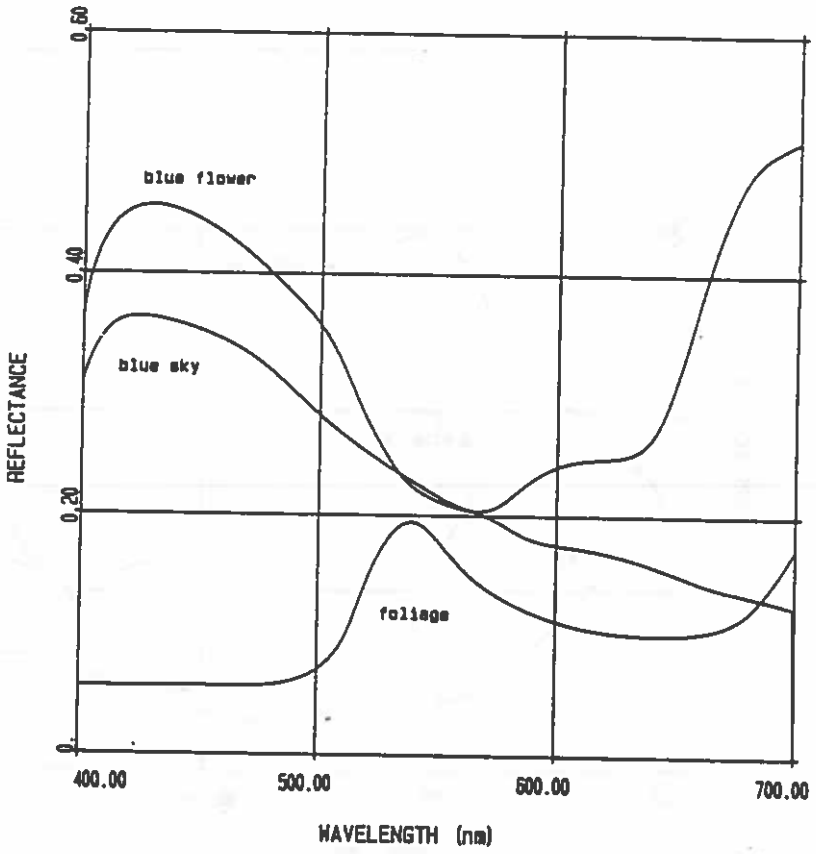

Figure 5b: Reflectances of the blue flower, blue sky, and foliage patches in the Macbeth ColorChecker chart (after [15]).

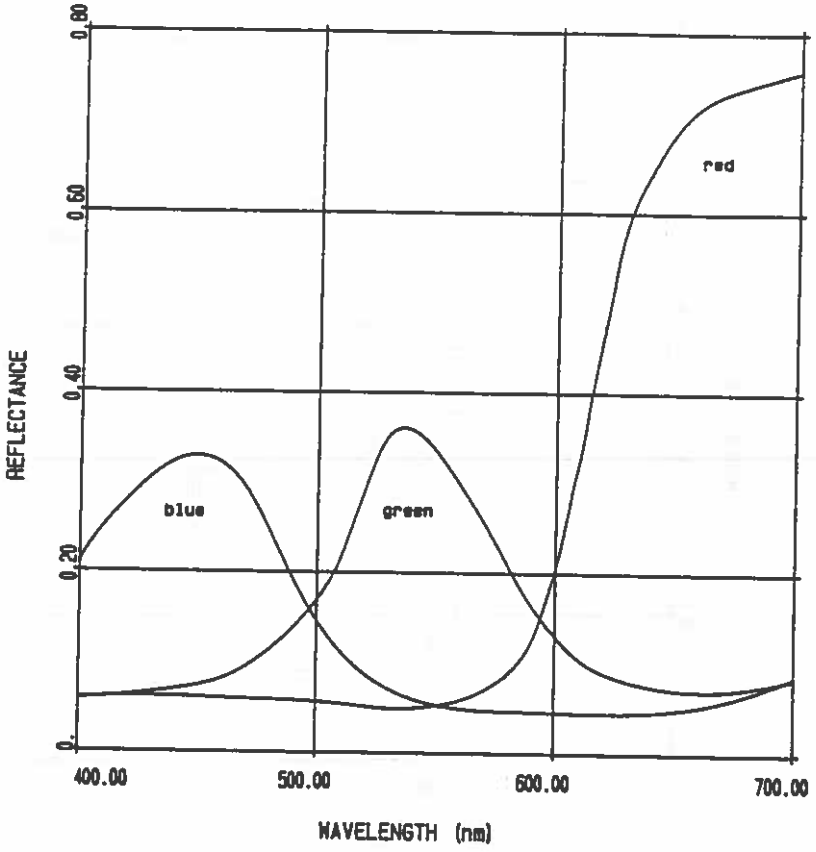

Figure 5d: Reflectances of the blue, green, and red patches in the Macbeth ColorChecker chart (after [15]).

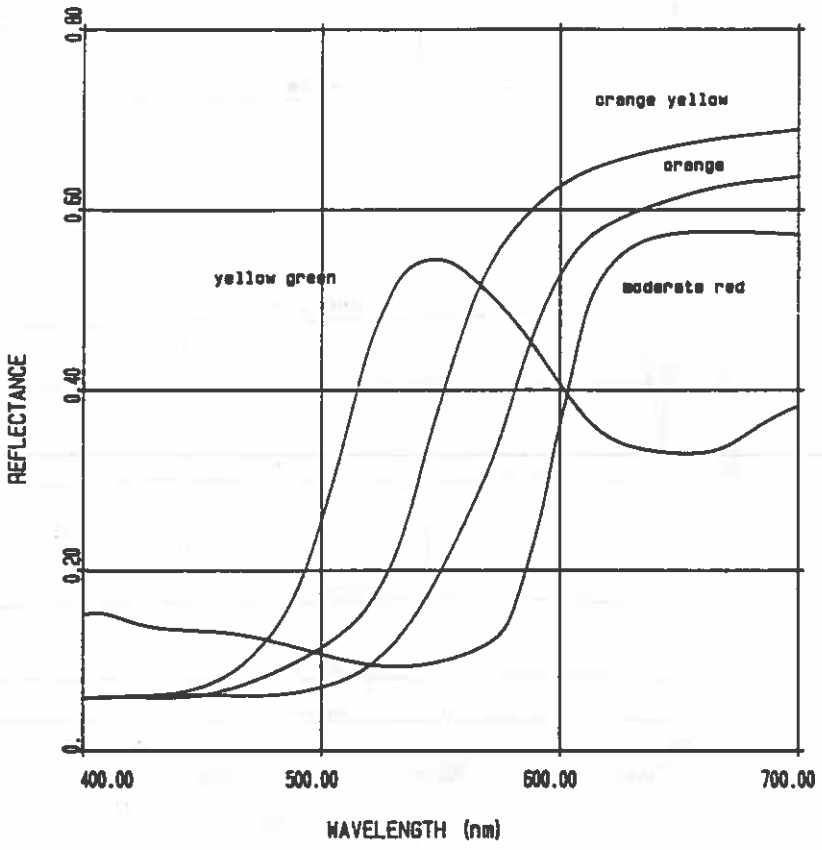

Figure 5f: Reflectances of the yellow green, orange yellow, orange, and moderate red patches in the Macbeth ColorChecker chart (after [15]).

using Eqs. (13) and (16a). For each color space the average color error per patch of the Macbeth Color Checker chart was determined for every possible combination of integration order. The results from those combinations which employed the same total number of wavelengths were then averaged. This was done to eliminate the importance of any one of the components of a tristimulus value and to accomodate the fact that certain combinations of integration order for SML and CIE XYZ space are undefined for AC_1C_2 space. The results for the three color spaces are shown in Fig. 6. At each level of computational expense as defined by the number of wavelengths employed, AC_1C_2 space is clearly superior to both CIE XYZ space and SML space.

The next test evaluated the relative importance of each component of the AC_1C_2 tristimulus values. A diagram was constructed from the data obtained by using all possible combinations of orders to compute AC_1C_2 tristimulus values for the color patches of the Macbeth chart. For each combination of orders, the number of wavelengths allocated to each component of the tristimulus value was divided by the total number of wavelengths used for all three components of the tristimulus value. This produced a fraction, analogous to a chromaticity coordinate, for each component. The three wavelength fractions for each data point were used to determine a position on an equilateral triangle. Locations near the corners of the triangle were cases where most of the wavelengths were used for just one of the three coordinates, positions near the edges of the triangle were cases where most of the wavelengths were used for just two of the three coordinates, and positions in the interior of the triangle were cases where there was a more even distribution of the wavelengths amongst all three of the coordinates. The triangle was discretized into smaller equilateral triangles and an average error, expressed as a distance in $L^*a^*b^*$ space, was computed for each sub-triangle from the data points that fell within the sub-triangle's boundaries. This

average error determined the height of a triangular bar positioned above the sub-triangle.

The diagram that results from the above procedure is shown in Fig. 7. Clearly the best results occur in the interior portions of the diagram where the wavelengths are distributed amongst all of the coordinates. However, in cases where more wavelengths are used for one coordinate than for the other two, smaller errors occur when the A coordinate is favored over the C_1 and C_2 coordinates. To a lesser extent, the C_1 coordinate is also to be preferred over the C_2 coordinate. These results are consistent with the prediction of the eigenvalue ratio given in Eq. (10).

The final test explored one specific approach to keeping the total number of wavelengths employed to an absolute minimum. This approach is based on the assumption that no matter how many wavelengths are used, one wavelength for each of the major peaks in the $\overline{a}(\lambda)$, $\overline{c}_1(\lambda)$, and $\overline{c}_2(\lambda)$ functions in Fig. 4 should be correctly determined. First order quadrature for the C_2 component and second order quadrature for the C_1 component requires the three wavelengths and weights given in Table 1a. This takes care of three of the major peaks and distributes the wavelengths between the C_1 and C_2 components in a manner consistent with the eigenvalue ratio and the results of the last test. Third order quadrature for the A component takes care of the fourth major peak and allocates the most wavelengths to the most important coordinate. The first row in Table 2 repeats from Table 1a the wavelengths and weights necessary to perform gaussian quadrature with this combination of orders. Also given is the average error in $L^*a^*b^*$ space when the tristimulus values of the Macbeth Color Checker chart are computed using these parameters.

Comparison of the wavelengths used for third order quadrature of the A component and second order quadrature of the C_1 component reveals that the two wavelengths used for the C_1 component are very close to two of the wavelengths used for the A component. If

A		C_1		C_2		$L^*a^*b^*$ error
λ_i	H_i	λ_i	H_i	λ_i	H_i	
483.0 557.7 632.3	0.15908 0.71695 0.18035	490.9 631.4	0.31824 -0.46008	456.4	0.54640	5.432
490.9 557.7 631.4	0.18892 0.67493 0.19253	490.9 631.4	0.31824 -0.46008	456.4	0.54640	5.429

Table 2: Results from using gaussian quadrature to compute the tristimulus values of the Macbeth Color Checker chart. In the second row, wavelengths from the C_1 component have also been used for the A component.

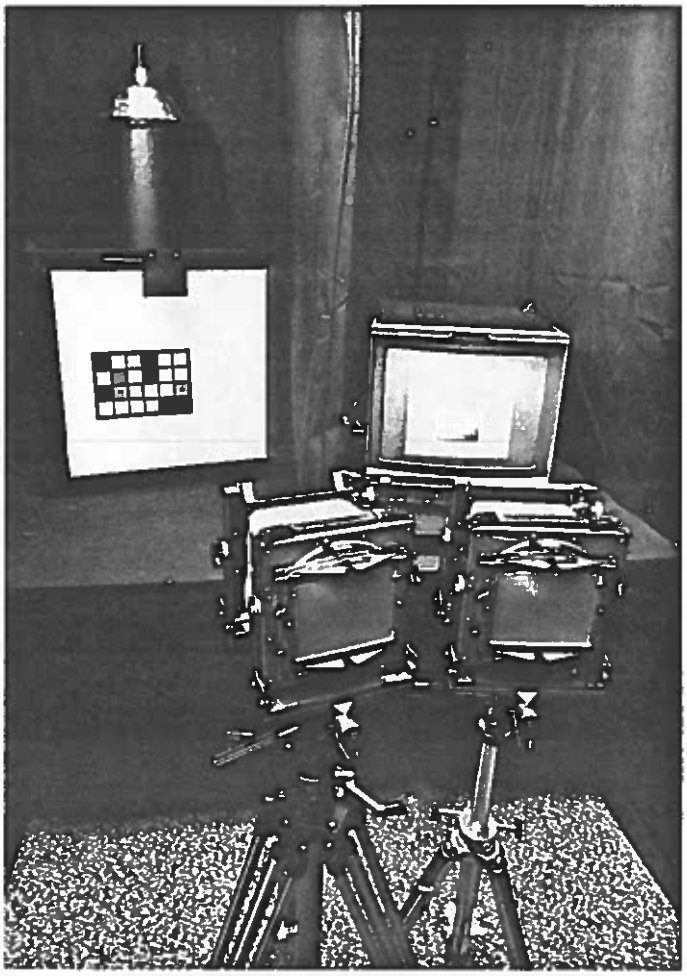

Figure 8: Experimental setup with partioning curtains removed.

produce the computer generated pictures. This technique is based on the assumption that the environment can be discretized and that each of the surfaces either emits or reflects in a pure diffuse (Lambertian) manner. An energy balance is performed on the environment and the radiosity of each surface is solved for. The calculations are performed on a wavelength basis. The resulting spectral energy distributions are resolved to tristimulus values and are displayed on a color television monitor.

The monitor had a 20-inch display tube with phosphor chromaticity coordinates:

$$\begin{aligned} x_r &= 0.64 \quad x_g = 0.29 \quad x_b = 0.15 \\ y_r &= 0.33 \quad y_g = 0.60 \quad y_b = 0.06 \end{aligned} \tag{18}$$

The individual brightness and contrast controls for each of the monitor guns were adjusted to yield a D6500 white point, and the individual gamma correction functions were measured for each of the guns. (The curves that were measured were used as is with no attempt to fit them with a single power law curve.) The luminance ratios necessary to set the white point were found to be:

$$Y_r : Y_g : Y_b = 102.4 : 2.29 : 0.0221 \tag{19}$$

By determining the proportional relationship between luminance and radiance for each of the guns, these luminance ratios were converted to radiance ratios and were used to balance the guns over their entire dynamic range. The luminance of the white point was set to 24 foot lamberts.

Two 4x5 view cameras were used to view the model and the monitor. Fresnel lenses were placed in front of the ground glass of each camera to act as image intensifiers. The combination of f-stop setting and camera to model distance were such that the entire depth of the model was in focus thereby minimizing depth of field problems. The images, as seen by the subjects, were inverted.

a brief set of instructions and a series of three questions. For the test the subjects were told that the real model was on the left and the computer generated image was on the right. Two of the questions involved A/B comparisons between the members of the two pairs of images described above. A third question asked for a rating of the color match between the real model and the image computed using only four wavelengths.

In addition to the instructions on the questionnaire each subject was also given some verbal instructions before taking the test. First the chair was adjusted so that each person's head was in roughly the same position. Then they were told not to lean forward to get closer to the view cameras or to turn their head from side to side. All evaluations were to be made by shifting the gaze from one view camera to another.

The results of the experiment are given in Table 3. When the images were computed using different fundamentals but the same number of wavelengths for each component of the tristimulus values, the subjects showed a clear preference for the image produced using the AC_1C_2 fundamentals over the image produced using the SML fundamentals. The sign test indicates that this result is significant at the .05 confidence level. The order of presentation of the two images can be shown by Fisher's exact test to have had no significant effect. When the AC_1C_2 fundamentals were used to compute the tristimulus values for each image but the number of wavelengths allocated for each AC_1C_2 component was varied, the image where more wavelengths were allocated to A was clearly preferred to the image where more wavelengths were allocated to C_1. Once again, the sign test indicates that this result is significant at the .05 confidence level while Fisher's exact test shows that order of presentation had no significant effect. Finally, the color match between the real model and the image computed using the AC_1C_2 fundamentals and a total of four wavelengths was rated as being good.

5. Summary and Conclusions

This paper has shown how gaussian quadrature can be used with a set of opponent fundamentals to select the wavelengths at which to perform synthetic image generation. The fundamental human spectral sensitivity functions were introduced and were expressed in terms of the CIE XYZ matching functions. The Karhunen-Loeve expansion was used to transform these functions into a set of opponent fundamentals. Gaussian quadrature with the opponent fundamentals as weighting functions was used to select wavelengths for realistic image synthesis. The spectral reflectances of the Macbeth Color Checker chart were used to evaluate the technique. This was accomplished through color difference calculations and a perceptual comparison experiment.

It can be concluded that an opponent color space, such as AC_1C_2 space, has important properties for realistic image synthesis. Better color accuracy is achieved with fewer wavelengths when the wavelengths are selected based on AC_1C_2 space than when they are chosen using either CIE XYZ space or $SM\dot{L}$ space. Within AC_1C_2 space itself, the A coordinate is most important, the C_1 coordinate is second most important, and the C_2 coordinate is least important. This information can be used to select wavelengths for synthetic image generation and leads to a particularly efficient four wavelength set that roughly corresponds to the four peaks of the opponent fundamentals themselves.

The primary area for future work is to extend the wavelength selection techniques to discontinous spectral energy distributions. This would avoid the situation where the peaks of a "spikey" spectral energy distribution lie between the wavelengths selected to perform the simulation. Some type of pre-filtering of the spectral energy distribution should overcome this problem.

a technique developed by Vos and Walraven [23] and Walraven [24]. Based primarily on the assumption that the nerve signals must be balanced in order for hue to remain constant with intensity at wavelengths 475.5 nm and 570 nm, and the assumption that the neural network which produces these signals has an opponents architecture, it is postulated in these articles that the following relations must hold for the fundamental spectral sensitivities $\overline{s}(\lambda)$, $\overline{m}(\lambda)$, and $\overline{l}(\lambda)$:

$$\begin{aligned} \frac{\overline{s}(475.5)}{\overline{m}(475.5)+\overline{l}(475.5)} &= \frac{1}{16} \\ \frac{\overline{l}(570.0)}{\overline{m}(570.0)} &= 2 \end{aligned} \tag{21}$$

This is shown to imply that the foveal cone receptors have effective population densities in the ratios $L : M : S := 32 : 16 : 1$. This correlates nicely with a receptor mosaic which has been shown to be hexagonal in pattern.

Given the 1931 CIE standard observer matching functions, the dichromatic chromaticity confusion loci in Eq. (20), and the ratios of Eq. (21), the definition of the fundamental spectral sensitivities given in Eq. (1) can be derived as shown in Wyszecki and Stiles [25]. It is important to note that there are limitations to the accuracy of the 1931 CIE standard observer and that there are alternative color matching data available. The accuracy of the data was limited because brightness matching had to be substituted for radiometric measurements due to the limitations of the technology available in 1931. There have also been corrections to the photopic luminous efficiency function since that time which would change the definition of the standard observer's $\overline{y}(\lambda)$ matching function. In 1952, Stiles and Burch [26,27] used modern instrumentation to perform the color matching experiments again. Estevez [22] has recommended the use of these color matching functions in lieu of the 1931 CIE standard observer. However, in this paper the standard observer data is employed because certain colorimetric data (like the chromaticity coordinates of phosphors) is only

Acknowledgements

Professor Donald P. Greenberg supervised this research from its inception. Help in performing the statistical analysis was provided by Professor Thomas Gilovich. Holly Rushmeier and Michael Cohen helped construct the equipment for the comparison experiment and assisted in conducting the tests that were involved. Michael also wrote the radiosity software that was used to produce the pictures that were used in these experiments. This work was performed under partial funding by National Science Foundation grant DCR-8203979, "Interactive Computer Graphics Input and Display Techniques."

References

[1] R. L. Cook and K. E. Torrance. A reflectance model for computer graphics. *ACM Transactions on Graphics*, 1:7–24, 1982.

[2] Roy A. Hall and Donald P. Greenberg. A testbed for realistic image synthesis. *IEEE Computer Graphics and Applications*, 3:10–20, 1983.

[3] G. Buchsbaum and A. Gottschalk. Trichromacy, opponent colours coding and optimum colour information transmission in the retina. *Proceedings of the Royal Society of London, Series B*, 220:89–113, 1983.

[4] A. Gottschalk and G. Buchsbaum. Information theoretic aspects of color signal processing in the visual system. *IEEE Transactions on Systems, Man and Cybernetics*, SMC-13:864–873, 1983.

[5] Keinosuke Fukunaga. *Introduction to Statistical Pattern Recognition.* Academic Press, New York, 1972.

[16] CIE recommendations on uniform colour spaces, colour-difference equations, and psychometric colour terms. Supplement No. 2 to Publication CIE No. 15, *Colorimetry* (E-1.3.1) 1971, Bureau Central de la CIE, Paris, 1978.

[17] Gary W. Meyer, Holly E. Rushmeier, Michael F. Cohen, Donald P. Greenberg, and Kenneth E. Torrance. An experimental evaluation of computer graphics imagery. *ACM Transactions on Graphics*, 5, 1985.

[18] C. Goral, K. E. Torrance, D. P. Greenberg, and B. Battaile. Modeling the interaction of light between diffuse surfaces. *Computer Graphics*, 18:213–222, 1984.

[19] M. Cohen and D. P. Greenberg. The hemi-cube: a radiosity solution for complex environments. *Computer Graphics*, 19:31–40, 1985.

[20] W. B. Cowan. An inexpensive scheme for calibration of a colour monitor in terms of the cie standard coordinates. *Computer Graphics*, 17:315–321, 1983.

[21] G. Meyer and D. P. Greenberg. Perceptual color spaces for computer graphics. *Computer Graphics*, 14:254–261, 1980.

[22] O. Estevez. *On the fundamental data-base of normal and dichromatic color vision.* PhD thesis, University of Amsterdam, Amsterdam, 1979. Krips Repro Meppel.

[23] J. J. Vos and P. L. Walraven. On the derivation of the foveal receptor primaries. *Vision Research*, 11:799–818, 1970.

[24] P. L. Walraven. A closer look at the tritanopic convergence point. *Vision Research*, 14:1339–1343, 1974.

[25] G. Wyszecki and W. S. Stiles. *Color Science: Concepts and Methods, Quantitative Data and Formulae.* John Wiley and Sons, New York, second edition, 1982.